

J.F. EBLE
F. SCHMIDT-KALER 

Optimization of frequency modulation transfer spectroscopy on the calcium 4^1S_0 to 4^1P_1 transition

Institut für Quanteninformationsverarbeitung, Universität Ulm, Albert-Einstein-Allee 11,
89069 Ulm, Germany

Received: 23 August 2006/Revised version: 19 April 2007
© Springer-Verlag 2007

ABSTRACT We present experimental results of frequency modulation transfer spectroscopy in a vapor of neutral atomic calcium. The observed line shapes agree well with the theoretical model. We use numerical calculations in order to improve the signal shape such that its magnitude and its slope at the zero-crossing is maximized. When optimized this way, the frequency modulation transfer signal can be used for the sensitive optical detection of rare species or isotopes, Doppler-free frequency measurements or as a sensitive error signal for laser frequency stabilization.

PACS 42.62.Fi; 32.70.Jz; 39.30.+w


1 Introduction

The aim of this paper is to systematically improve the frequency modulation transfer spectroscopy signal such that its magnitude and its slope near the zero-crossing are optimal. Parallel to the experiment, we obtain a set of parameters via numerical simulations, and compare experimental data and numerical results quantitatively. This procedure is shown here for the atomic transition $4^1S_0 \leftrightarrow 4^1P_1$ of neutral calcium vapor near 423 nm but is easily applied for any transition or element. Doppler-free spectroscopical methods are used to suppress the line broadening caused by the atomic velocity distribution. Commonly used techniques are saturation spectroscopy [1], polarization spectroscopy [2] and multi-photon spectroscopy [3].

Frequency modulation transfer spectroscopy (FMTS) is a subtype of saturation spectroscopy techniques and is mainly applied to detect atomic or molecular transitions with high accuracy [4–6]. A pump beam is phase modulated and transmitted through an atomic vapor probe. The counter-propagating probe beam is observed after transmission through the vapor. Due to a non-linear four-wave mixing process in the atomic sample the probe light acquires sidebands, and a transfer of modulation from pump to probe beam occurs. In the counter-

propagating alignment of both beams, the nonlinear effect happens only for atoms of the velocity class zero, such that no contribution from the thermal motion of the atoms in the vapor broadens the resonance line. More commonly used is frequency modulation (FM) spectroscopy [7]. In this case the probe beam is modulated before the passage through the sample and a counter-propagating unmodulated saturation beam is sent in. It can be shown that even in the Doppler free resonance of the FM a contribution of the thermally broadened atomic velocity distribution remains. Here lies an advantage of the FMTS technique over the FM technique, since only atoms or molecules of velocity class zero contribute to the non-linear four-wave mixing signal. Therefore, FMTS does show a fully Doppler free signal, holding some advantages for applications such as an error signal to lock a laser precisely to a well-known atomic transition. This spectroscopic technique is also used in applications for Bose–Einstein condensation and quantum information processing where the knowledge of the exact atomic transition frequency or a precisely fixed laser frequency is essential. Our application regards the frequency stabilization of a laser for photo-ionization in order to load ion traps. We stabilize a laser to the calcium transition $4^1S_0 \leftrightarrow 4^1P_1$ near 423 nm, which serves as the first excitation step to selectively generate isotopes of Ca^+ -ions. The second ionization step uses laser light near 374 nm [8], see also [9]. Furthermore, the FMTS signal has been used to calibrate a high-precision wavemeter and to characterize its long-term stability.

The paper is focused on the quantitative comparison between the experimental and theoretical optimization of the FMTS signal and is organized as follows. In Sect. 2 we describe the experimental setup. It can be used to obtain a FMTS signal, or alternatively for regular saturation spectroscopy if the modulation of the pump beam is switched off. In a first step we test the setup and record the linewidth of the calcium transition with saturation spectroscopy. Then we describe and characterize the modulation of the pump beam. A brief review of the theoretical description of the FMTS spectroscopy follows. In Sect. 3 our numerical signal optimization is outlined resulting in a strategy to improve the FMTS signal line shape. To validate the simulations, we compare the numerical results in Sect. 4 with the measured signals based on the previous characterization of the electro optical modulator.

 Fax: +49-731-5022839,
E-mail: ferdinand.schmidt-kaler@uni-ulm.de

2 Experimental setup

2.1 Spectroscopic arrangement

In the experiment, we start with the beam near 423 nm emerging from a frequency doubling laser system¹. The beam is divided with a combination of a half-wave plate and a polarizing beam splitter in a pump and a probe beam with an intensity ratio of 70 : 30. For FMTS the pump beam can be modulated with an electro-optical modulator² (EOM) made of a LiNbO₃ crystal, with dimensions of width 3 mm, height $h = 3$ mm, and length $l = 60$ mm. The crystal is gold coated on the top and on the bottom surfaces, serving as contact electrodes, which are connected to an oscillator with modulation frequency $\omega_M/(2\pi) = 23.7$ MHz. This frequency has been chosen³ according to the condition $\omega_M/(2\pi) = 0.7\gamma$ [4]. The applied voltage $U(t) = U_0 \cos(\omega_M t)$ is enhanced by an electrical resonance circuit consisting of the EOM crystal as a capacitor and a ferrite inductor. A voltage amplification factor of 15.8 ± 0.2 has been determined.⁴ The circuit has been tuned such that the resonance frequency matches with ω_M and the electrical coupling is impedance matched to 50 Ω . Radio-frequency power and frequency applied to the EOM resonance circuit can be varied.

To vaporize solid calcium we use a sealed cell similar to the construction described in [11, 12]. The cell consists of a steel tube of length 500 mm with radius 18 mm that is closed with removable CF-windows on each side to enable filling with calcium metal grains. First, the gas in the cell is pumped to a pressure of $p \leq 10^{-5}$ mbar. The calcium vapor pressure is controlled by heating the tube to about 400 °C with a heating element⁵ fixed to the mid surface of the tube. All hot parts of the vapor cell are covered by a thermal insulation material.⁶ Stable operation of the cell up to 600 °C has been observed but is not necessary [10] in our experiments, as the atomic gas becomes fully opaque above 430 °C [12].

Lenses focus the counter-propagating and overlapping probe- and pump-beam to a waist of $w \sim 160$ μm at the center of the vapor cell. Four-wave mixing in the calcium vapor transfers modulation sidebands from the pump- to the probe-beam at integer multiples of the modulation frequency. The probe light that is transmitted through the cell now contains modulation sidebands at frequencies $\omega_{\text{laser}} \pm n\omega_M$ and is detected by a fast photodiode⁷, the photo current is mixed with a local oscillator at frequency ω_M on a phase detector⁸. Subsequently high frequency components in the electrical signal are filtered out by a low pass filter with cut off frequency $f_{(-3 \text{ dB})} = 2.5$ MHz.

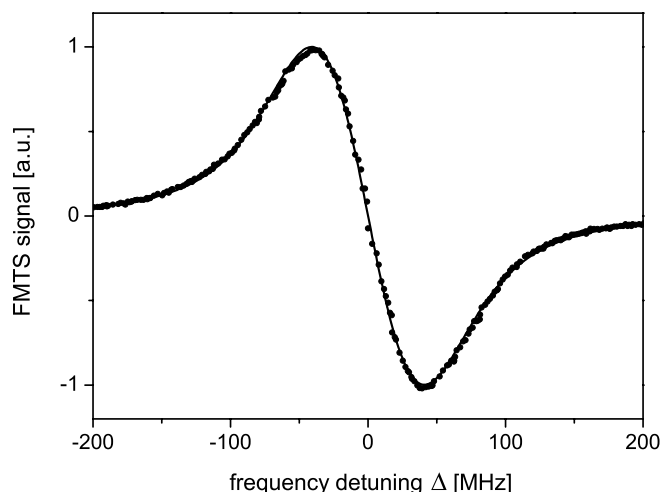


FIGURE 1 Measured (dots) and calculated (line) FMTS signal with optimized settings. For the theoretical line shape we use the values of $\beta = 2.61$, $\varphi = 0.75\pi$ and $\gamma = 60$ MHz. The data acquisition time per point corresponds to 20 Hz and the full scan is taken in 20 s

If the laser frequency is tuned across the calcium transition the FMTS signal shape is obtained. We control the laser detuning via the piezo-electrically driven Littrow grating angle of the diode laser by the analog output of a PC card. The PC also reads the FMTS signal and the actual wavelength with a Fizeau wavemeter⁹. By simultaneously recording wavelength and FMTS voltage the line shape can be directly plotted (Fig. 1). As the computer data acquisition rate is limited in our case by the PCI card of the wavemeter to about 20 Hz we additionally filter high frequency noise from the FMTS signal by a 150 Hz lowpass filter. Under typical operation conditions and with ~ 3 mW of laser power we observe a signal to noise ratio of 180. If used as an error signal for frequency stabilization, the noise limited stability would be 140 kHz within a 150 Hz detection bandwidth (corresponding to 12 kHz/ $\sqrt{\text{Hz}}$).

2.2 Measurement of line broadening effects

To analyze line broadening effects we investigate saturation spectroscopy with our setup. The pump-beam amplitude is modulated by an optical chopper at a frequency of 218 Hz and the probe-beam signal is phase sensitively amplified with a lock-in amplifier¹⁰. We expect the saturated absorption dip resonance to be widened not by collisions or transit-time broadening, but by saturation broadening. The linewidth broadened in such a way reads as

$$\gamma_S(I) = \gamma \sqrt{1 + I/I_{\text{Ref}}}, \quad (1)$$

with the laser intensity I and a reference saturation intensity corresponding to the convention that $I = I_{\text{Ref}}$ for $\Omega_{\text{Rabi}} = \gamma$.

The insert of Fig. 2 shows a lock-in signal of the saturated absorption signal at a laser power of 0.15 mW. If we plot the linewidth of the absorption signals as a function of laser power, as shown in Fig. 2, the power broadening of the signal is clearly observed. With proper weighting of error bars

¹ DL-SHG 110 (Toptica Photonics)

² Lithium niobate (Deltronic Crystal Industries)

³ For the setup of the experiment we followed this advice from literature. At the end of Sect. 3 of this paper we discuss the limitations of the argument.

⁴ For the electrical measurement of the amplification by the resonance circuit we used two passive probe heads, one before and after the LC resonator circuit. To minimize errors due to slight differences in the probes, the probe heads have been swapped once.

⁵ SEI 20/200 (Thermocoax)

⁶ WDS-shape (Porextherm)

⁷ Model 1801 visible DC-125 MHz low noise photoreceiver (New Focus)

⁸ ZSC-2-1W (Mini-Circuits)

⁹ WS Ultimate (HighFinesse-Angstrom)

¹⁰ model 5209, EG&G Princeton

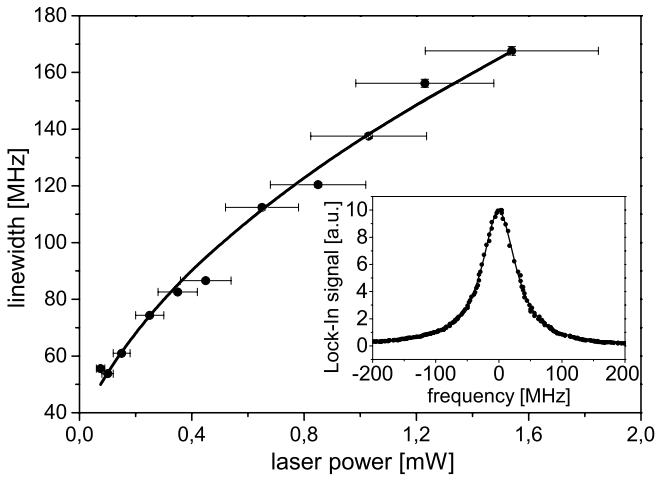


FIGURE 2 Linewidth of the power broadened dip of the saturated absorption as a function of the sum of the pump and probe laser power. *Insert:* Lock-in signal of the absorption signal

in the laser power¹¹ and the widths of the absorption signals we deduce a linewidth of $\gamma/(2\pi) = 34.4(5.3)$ MHz from the fit, in good agreement with the measured value of $\gamma/(2\pi) = 34.6(1.5)$ MHz reported in [15] and calculated in [16]. Our calculated saturation reference intensity is 120 mW/cm^2 . If we reveal a saturation reference intensity from the slope of Fig. 2, this leads to a value that is about 25% off the expected one. This can be explained by a non gaussian laser beam shape which leads to an inaccuracy in the beam waist determination.¹²

2.3 Characterization of the electro-optical modulator

After having tested the optical experimental setup by regular saturation spectroscopy we focus on the characterization of the EOM. For a quantitative comparison between the experimental FMTS signal and the corresponding theoretical expectation, the precise knowledge of the modulation index is of importance. In the following, we determine the modulation index for the EOM crystal both theoretically and experimentally.

For phase modulation, a linear relation between the voltage¹³ V applied to the EOM-crystal and the corresponding modulation index β is predicted. In our setup, we use a rectangular LiNbO_3 crystal cut with its input and output facets parallel to the xz -plane of the crystals principal axes and with the electrical modulation field applied parallel to the z -direction, upper inset of Fig. 3. The polarization of the light is aligned along the z -axis. For this geometry the modulation is given by [17]

$$\beta(V) = \frac{\pi l}{\lambda} n_e^3 r_{33} \frac{V}{h}, \quad (2)$$

¹¹ The error bars of the laser power are dominated by the laser diode feed-forward regulation that alters the laser diode current during the frequency scan of the grating piezo. Therefore, the laser power varies during the frequency scan. The plotted power values have been measured close to the atomic resonance frequency near $\Delta \sim 0$.

¹² WM100 (Thorlabs)

¹³ The voltage U is measured as half the peak-to-peak value

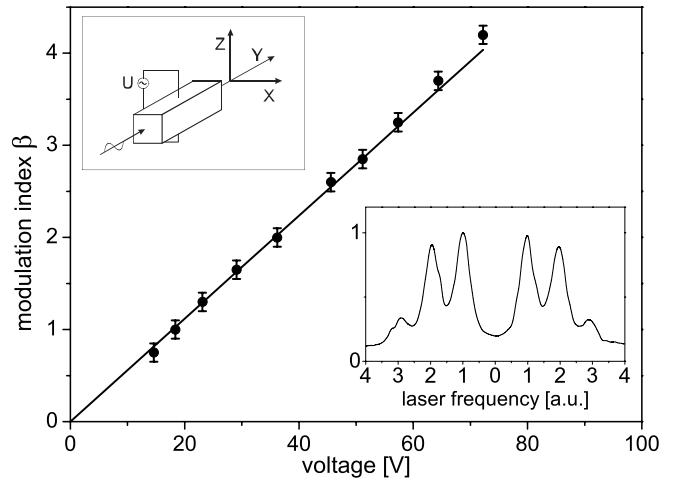


FIGURE 3 Modulation index β vs. modulation voltage V applied at the EOM crystal. *Solid line:* theoretical determined dependence from the LiNbO_3 crystal properties, no fit to the data. *Dots:* experimental result for β determined from heights of the modulation sidebands measured in the cavity transmission spectra. *Upper inset:* geometry of the modulation crystal and light. *Lower inset:* recorded example of a cavity transmission spectrum with sidebands, with the carrier being suppressed for the specific value of $\beta = 2.6$

where λ is the wavelength of the laser light, l is the length and h the height of the crystal. The relevant electro-optic coefficient is $r_{33} = 30.8 \text{ pm/V}$ [17]. The extraordinary index of refraction can be evaluated for the wavelength of 423 nm using a Sellmeier equation [18], yielding the value of $n_e = 2.30$ at $T = 22^\circ \text{C}$. The theoretical dependence of the modulation index β as a function of the applied voltage V is drawn as a line in Fig. 3 ($\beta = 0.056 \text{ V}$).

In order to verify this relation for the modulation index experimentally, we analyze the phase modulated light. For this, the beam is coupled into a cavity of finesse $F = 111(3)$ with a free spectral range of 1.5 GHz . The transmitted intensity is observed while detuning the laser frequency over the cavity resonance. The light field of the modulated pump beam reads as

$$E(t) = \frac{E_0}{2} e^{i\omega t} \sum_{n=-\infty}^{\infty} J_n(\beta) e^{in\omega M t} + \text{c.c.} \quad (3)$$

Scanning the laser frequency allows the measurement of the sideband spectrum $|E(t)|^2$ with the height of the n -th sideband given by the squared Bessel function $J_n^2(\beta)$.

From the light field we extract the value of β from a fit with superimposed Lorentz functions. The experimental determination of the modulation index for a given voltage is plotted in Fig. 3. If we take into account the independently measured voltage enhancement factor of the LC circuit, the measured values of β agree with the theoretical expectation (2) and the corresponding voltage V .

Note that in the sideband spectrum $J_n^2(\beta)$ and $J_{-n}^2(\beta)$ are balanced with deviations smaller than 1% for $\beta < 2.5$. However, deviations $< 7\%$ appear in the height of the n -th sideband for $2.5 < \beta < 4.2$. Larger voltage amplitudes ($\beta < 4.2$) lead to a significant amplitude modulation disturbing the sideband configuration. An extensive discussion of the effect of residual amplitude modulation in the case of frequency mod-

ulation saturation spectroscopy is found in [19]. Also a FMSTS signal would become highly deformed under these conditions.

3 Theory of the FMSTS signal and its optimization

The FMSTS signal shape is evaluated in third-order perturbation theory with the restrictions to two-level atoms, steady-state solutions and plane wave fields [13, 14]. The photodiode generates from the probe beam a current signal proportional to the light intensity. The internal transimpedance amplifier converts the photo current to an output voltage U^{PD} .

$$U^{\text{PD}}(\Delta, t) = C \sum_{n=-\infty}^{\infty} J_n(\beta) J_{n-1}(\beta) \left[\left(L_{\frac{n+1}{2}}(\Delta) + L_{\frac{n-2}{2}}(\Delta) \right) \cos(\omega_M t + \varphi) + \left(D_{\frac{n+1}{2}}(\Delta) - D_{\frac{n-2}{2}}(\Delta) \right) \sin(\omega_M t + \varphi) \right], \quad (4)$$

with the auxiliary functions

$$L_n(\Delta) = \frac{\gamma^2}{\gamma^2 + (\Delta - n\omega_M)^2} \quad (5)$$

and

$$D_n(\Delta) = \frac{\gamma(\Delta - n\omega_M)}{\gamma^2 + (\Delta - n\omega_M)^2}, \quad (6)$$

which describe absorptive and dispersive contributions for the sidebands and the carrier $n = 0$. $\Delta = \omega_{\text{laser}} - \omega_0$ denotes the frequency detuning of the light field from the atomic resonance frequency, γ is the linewidth of the considered transition, $J_n(\beta)$ are the Bessel functions of n -th order with the modulation index β , and φ describes the relative phase between the signal voltage $U^{\text{PD}}(\Delta, t)$ and the local oscillator $U(t) = U_0 \cos(\omega_M t)$ of the same frequency. A constant C subsumes parameters such as the photodiode detection efficiency, photodiode transimpedance gain, laser light intensity, and laser beam attenuation by the cell. The phase detector mixes the photodiode signal U^{PD} with the voltage from the local oscillator $U(t)$ yielding the output:

$$S_{\beta, \varphi}(\Delta) = U^{\text{PD}}(\Delta, t) U_0 \cos(\omega_M t). \quad (7)$$

By considering only the time dependent trigonometric parts in (4) a time-independent term and a fast rotating term, respectively, are created

$$\cos(\omega_M t + \varphi) \cos(\omega_M t) = \frac{1}{2} (\cos(\varphi) + \cos(2\omega_M t + \varphi)), \quad (8)$$

and equivalently for the sines. The emerging DC terms are depending only on the phase φ and represent the FMSTS signal. Fast rotating terms at frequency $2\omega_M$ would disturb the signal and are filtered out with a 1.9 MHz lowpass.¹⁴ Hence, in the simulations we regard the signal with the following line shape

$$S_{\beta, \varphi}(\Delta) = C' \sum_{n=-\infty}^{\infty} J_n(\beta) J_{n-1}(\beta) \times \left[\left(L_{\frac{n+1}{2}}(\Delta) + L_{\frac{n-2}{2}}(\Delta) \right) \cos(\varphi) + \left(D_{\frac{n+1}{2}}(\Delta) - D_{\frac{n-2}{2}}(\Delta) \right) \sin(\varphi) \right]. \quad (9)$$

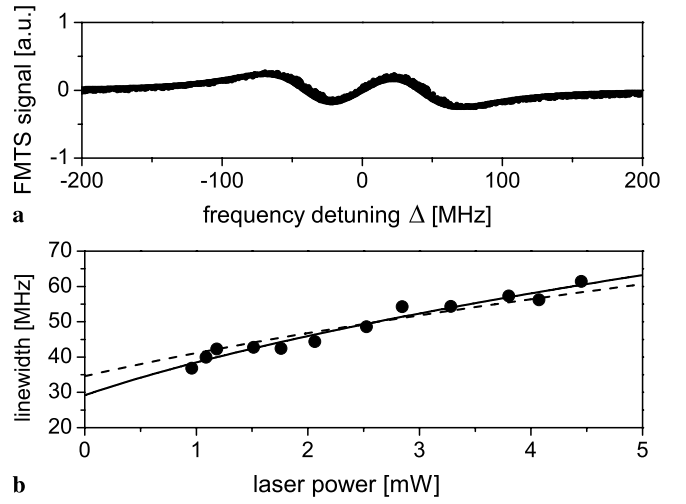


FIGURE 4 (a) Measured (*dots*) and calculated (*line*) FMSTS signal with unoptimized settings: $\beta = 3.00$ and $\varphi = 1.31\pi$, $\gamma = 34.7$ MHz. The scan parameters are identical to those in Fig. 1. (b) Linewidth of the FMSTS signal as a function of sum of the pump and probe laser power. The *solid line* displays (1) with both parameters fitted, yielding $\gamma \simeq 29.2$ MHz (*solid line*). The *dashed line* results if the linewidth is fixed to the literature value of $\gamma = 34.7$ MHz

For a very low modulation index β , the summation of Bessel functions reduces to the carrier and the first order sidebands and results in the familiar expression for the FMSTS signal [4, 13]. However, (9) includes all sidebands with the corresponding weighting of the Bessel functions [14]. Here, the beat-notes between all adjacent Bessel sidebands contribute to the photodiode signal U^{PD} . In the parameter range of our experiment, sidebands with $|n| > 10$ are so far detuned from the atomic absorption line that their contribution to the signal can be fully neglected for the numerical evaluation of (9). Typical signals are plotted in Figs. 1 and 4 together with measured data. The proportionality factor C' , including C but also the phase detector characteristics, the modulation index β and the linewidth¹⁵ γ are fitted to the data. A slight nonsymmetric behavior of the signal in Fig. 4 might be caused by the slightly unbalanced sideband structure (see also Sect. 2.3).

The effect of power broadening can also be observed on the FMSTS signal. Therefore, we record FMSTS signals for different laser intensities while all other parameters such as the modulation index, modulation frequency, cell temperature, and alignment of the laser beams are kept constant. The theoretical line shape (9) is fitted to those signals to extract a power broadened linewidth. These results are plotted in Fig. 4b as a function of the laser power. Using a saturation function (1) to fit the data, an extrapolated linewidth close to 30 MHz is found. The experimental findings fit almost equally well using $\gamma = 34.6$ MHz (dashed).

The purpose of the following numerical simulations is to identify the optimal setting for the parameters β and φ to

¹⁵ As in the regular saturation spectroscopy, the FMSTS signal might be saturation broadened for the laser power of ~ 3 mW. However, a direct comparison to I_{Ref} is not possible because the modulation of the pump beam with $\beta = 3$ leads to large spectral components of the pump beam outside the atomic resonance.

¹⁴ BLP-1.9 (Minicircuits.)

obtain a large FMTS signal with a steep slope in the zero-crossing of the signal. We start out with the magnitude of the signal,

$$M_{\beta,\varphi} = \max(S_{\beta,\varphi}(\Delta)) \quad (10)$$

being evaluated for φ and β . Figure 5 displays the magnitude of the signal for $\varphi \in (0, 2\pi)$ and $\beta \in (0, 10)$. The optimal phase is $\varphi \approx 0.85\pi$ modulo multiples of π . The optimal modulation index is $\beta \approx 6$.

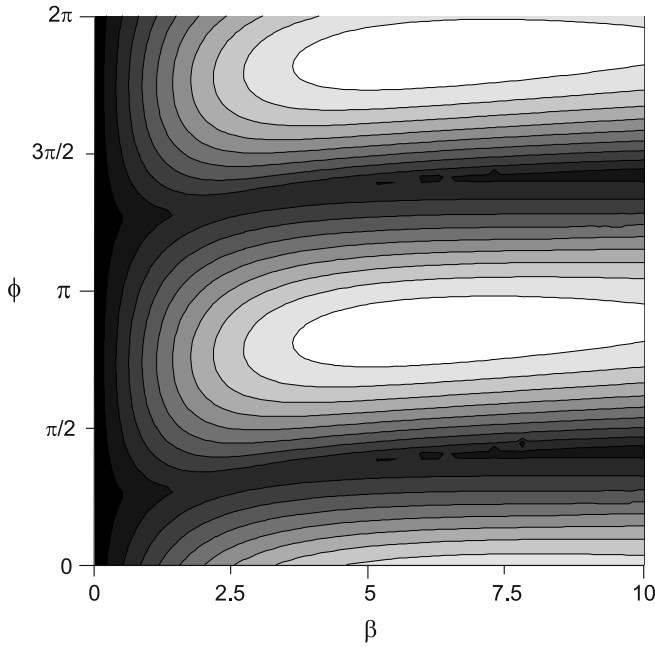


FIGURE 5 Magnitude $M_{\beta,\varphi}$ of the FMTS signal as a function of modulation index β and phase φ in a grayscale varying from small to big in black to white

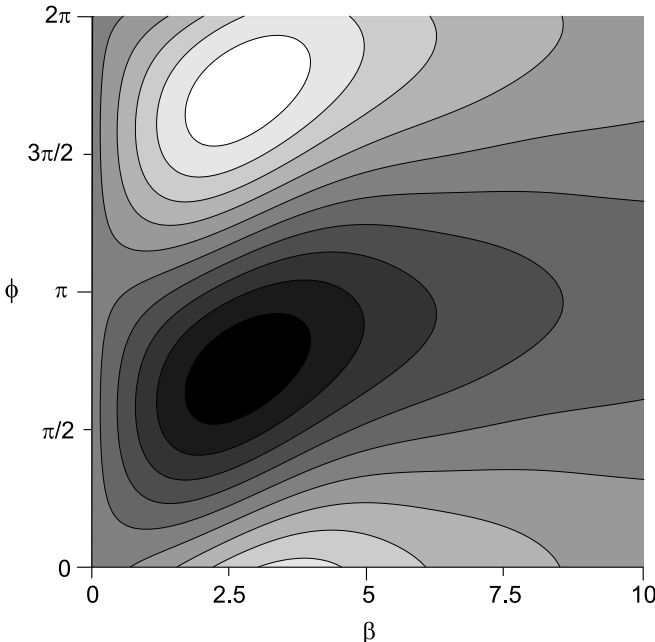


FIGURE 6 The derivative $D_{\beta,\varphi}$ in the zero crossing of the FMTS signal for varying modulation index β and phase φ

Second, the signal slope near the zero-crossing

$$D_{\beta,\varphi} = \left. \frac{\partial S_{\beta,\varphi}(\Delta)}{\partial \Delta} \right|_{\Delta=0} \quad (11)$$

is evaluated. Figure 6 shows the slope for $\varphi \in (0, 2\pi)$ and $\beta \in (0, 10)$ in a grayscale varying from the maximal positive derivative in white to the maximal negative derivative in black. The optimal modulation index is $\beta \approx 2.6$. The phase for a maximal negative slope is $\varphi \approx 0.7\pi$ and for a maximal positive slope $\varphi \approx 1.7\pi$, respectively. The optimization of $D_{\beta,\varphi}$ roughly agrees with that for $M_{\beta,\varphi}$ for values $\beta \simeq 3$ and $\varphi \simeq 0.7\pi$ with¹⁶ $\omega_M/(2\pi) = 0.7\gamma$. In general, combinations with $\omega_M/(2\pi) < \gamma$ and β can be evaluated that maximize $D_{\beta,\varphi}$. A lower ω_M is compensated by a higher value of β .

4 Measurements and comparison

In order to prove the agreement of $M_{\beta,\varphi}$ in simulations and experimental data we measured FMTS signals for various values of β . The phase was adjusted accordingly to a maximal signal height at $\beta = 2.6$ which corresponds to the negative derivative to $\varphi \approx 1.85\pi$. The measured magnitudes $M_{\beta,\varphi}$ are plotted in Fig. 7 normalized to a maximum value of one. The solid line represents a least-square fit in the vertical direction to data including the experimental errors in $M_{\beta,\varphi}$ and β to the theoretically expected function of (10).

The phase φ can be adjusted with different cable lengths between the photodiode and the phase detector. Fine adjustment of the phase is achieved by varying slightly the modulation frequency ω_M .

Similarly, the derivative $D_{\beta,\varphi}$ in the zero-crossing of the signal is investigated. Figure 8 shows the measured absolute values of $D_{\beta,\varphi_{\text{opt}}}$ together with the simulation, where the maximum of this curve is normalized to one. The fit of the data is performed as above. Again, we observe excellent agreement between the measurements and the simulation.

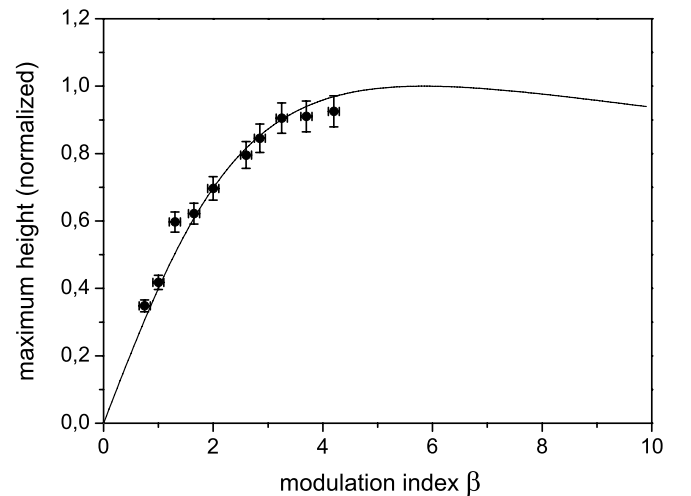


FIGURE 7 Comparison of measured and simulated FMTS signal magnitude $M_{\beta,\varphi_{\text{opt}}}$. The values for β are determined from the cavity transmission spectra

¹⁶ A choice of $\omega_M/(2\pi) = 0.7\gamma$ is motivated if in (9) only carrier and first order Bessel sideband are taken into account

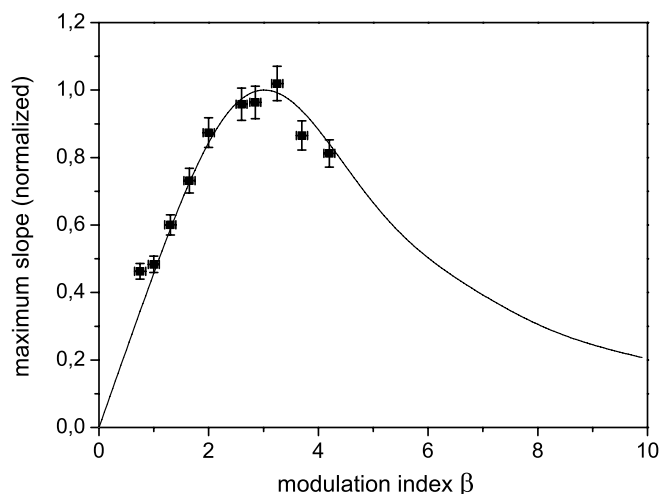


FIGURE 8 Comparison of measured and simulated derivatives $D_{\beta, \varphi_{\text{opt}}}$ in the zero-crossing of the FMST signal

5 Conclusion and outlook

Frequency modulation transfer spectroscopy signals appear in different shapes and magnitudes depending on the parameters modulation index β , and phase φ . We characterized the magnitude of the signal and its first derivative in the zero-crossing. Numerical simulations show a potential for improvement for both characteristic signal properties: searching weak atomic transitions we propose the choice of $\beta \approx 6$ and $\varphi \approx 0.85\pi$ for $\omega_M/(2\pi) = 0.7\gamma$. Determining the precise location of a transition frequency and locking a laser frequency to an atomic resonance will work best for $\beta \approx 2.6$ and $\varphi \approx 0.7\pi$. The theoretically obtained values have been confirmed very well by the experimental data.

In future, we will take advantage of the narrow dispersive FMST signal near 423 nm for the purpose of laser frequency stabilization. The second application will be the investigation of the long term stability of passive Fabry–Pérot reference cavities and of a wavemeter with a resolution in the range of 10^{-8} .

ACKNOWLEDGEMENTS We acknowledge financial support by the Landesstiftung Baden-Württemberg and the Deutsche Forschungsgemeinschaft. We thank V. Bendkowsky for her contributions in the early stage of the experiment and K. Singer for his constant support.

REFERENCES

- 1 W. Demtröder, *Laser Spectroscopy* (Springer, Heidelberg, 1996)
- 2 C. Wieman, T.W. Hänsch, *Phys. Rev. Lett.* **36**, 1170 (1976)
- 3 W. Kaiser, C.G. Garret, *Phys. Rev. Lett.* **7**, 229 (1961)
- 4 L.S. Ma, J.L. Hall, *IEEE J. Quantum Electron.* **QE-26**, 11 (1990)
- 5 L.S. Ma, P. Courteille, G. Ritter, W. Neuhauser, R. Blatt, *Appl. Phys. B* **57**, 159 (1993)
- 6 C. Raab, J. Bolle, H. Oberst, J. Eschner, F. Schmidt-Kaler, R. Blatt, *Appl. Phys. B* **67**, 683 (1998)
- 7 A.S. Zibrov, R.W. Fox, R. Ellingsen, C.S. Weimer, V.L. Velichansky, G.M. Tino, L. Hollberg, *Appl. Phys. B* **59**, 327 (1994)
- 8 S. Gulde, D. Rotter, P. Barton, F. Schmidt-Kaler, R. Blatt, W. Hogervorst, *Appl. Phys. B* **73**, 861 (2001)
- 9 A. Mortensen, J.J.T. Lindballe, I.S. Jensen, P. Staunum, D. Voigt, M. Drewsen, *Phys. Rev. A* **69**, 042502 (2004)
- 10 C.J. Erickson, B. Neyenhuis, D.S. Durfee, *Rev. Sci. Instrum.* **76**, 123 110 (2005)
- 11 M. Bacher, Diploma thesis, University Innsbruck, unpublished (2005)
- 12 J.F. Eble, Diploma thesis, University Ulm, unpublished (2006)
- 13 J.H. Shirley, *Opt. Lett.* **7**, 11 (1982)
- 14 E. Jaatinen, *Opt. Commun.* **120**, 91 (1995)
- 15 W. Hansen, *J. Phys. B* **16**, 2309 (1983)
- 16 J. Mitroy, *J. Phys. B At. Mol. Opt.* **26**, 3703 (1993)
- 17 A. Yariv, P. Yeh, *Optical Waves in Crystals* (Wiley, New York, 1984)
- 18 V.G. Dmitriev, G.G. Gurzadyan, D.N. Nikogosyan, *Handbook of Nonlinear Optical Crystals* (Springer, Berlin, 1991)
- 19 R. Wynands, A. Nagel, *J. Opt. Soc. Am. B* **16**, 10 (1999)